Research Square

Preprints are preliminary reports that have not undergone peer review.
They should not be considered conclusive, used to inform clinical practice,
or referenced by the media as validated information.

Bioinspired Design of Proximal Amine Boosts Electrocatalytic Reduction of CO 2 by Cobalt Tripyridine-Diamine Complex

Yong Yang

yangyongself@hzu.edu.cn

Huizhou University

Yuyang Fang

Huizhou University

Haofeng Wu

Huizhou University

Yanling Yao

Huizhou University

Ming Lu

Huizhou University

Zhaokai Zheng

Huizhou University

Yaxin Lian

Huizhou University

Jianing Jing

Huizhou University

Guocong Liu

Huizhou University

Jing Yang

Shenzhen Technology University

Huimin Yuan

City College of Huizhou

Research Article

Keywords: Cobalt complex, Second coordination sphere, Electrocatalysis, CO2 reduction

Posted Date: November 17th, 2026

DOI: https://doi.org/10.21203/rs.3.rs-11539732/v1

License: This work is licensed under a Creative Commons Attribution 4.0 International License.
Read Full License

Additional Declarations: No competing interests reported.

Bioinspired Design of Proximal Amine Boosts Electrocatalytic Reduction of CO_2 by Cobalt Tripyridine-Diamine Complex

Yong Yang,*[a] Yuyang Fang,[a] Haofeng Wu,[a] Yanling Yao,[a] Ming Lu,[a] Zhaokai Zheng,[a] Yaxin Lian,[a] Jianing Jing,[a] Guocong Liu,[a] Jing Yang,*[b] and Huimin Yuan*[c]

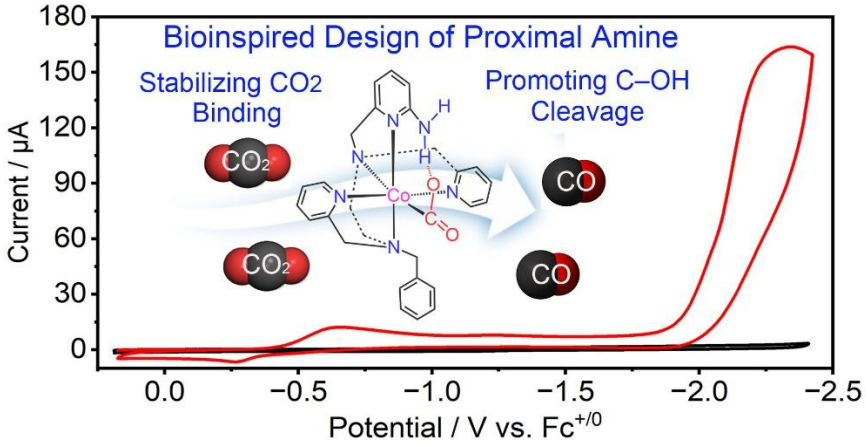
[a] School of Chemistry and Materials Engineering, Huizhou University, Huizhou, 516007, China

[b] College of Health Science and Environmental Engineering, Shenzhen Technology University, Shenzhen, 518118, China

[c] School of Intelligent Manufacturing, City College of Huizhou, Huizhou, 516007, China

*Corresponding author. E-mail address: yangyongself@hzu.edu.cn (Dr. Y. Yang); yangjing2@sztu.edu.cn (Dr. J. Yang); yuanhuimin@tm.hzc.edu.cn (Dr. H. Yuan)

Abstract: A bioinspired cobalt tripyridine–diamine complex (**Co-NH$_2$**) bearing an intramolecular secondary amine in the second coordination sphere was designed to mimic the hydrogen-bonding function of enzymatic active sites. A methyl-substituted analogue (**Co-CH$_3$**) was prepared as a control to probe the role of the pendant amine. Electrochemical measurements reveal that **Co-NH$_2$** exhibits higher catalytic current for CO_2 electroreduction relative to **Co-CH$_3$** in methanol-containing CO_2-saturated acetonitrile. Controlled-potential electrolysis confirms that CO and H_2 are the main products, with **Co-NH$_2$** achieving a CO Faradaic efficiency of 57% after 30 min, about twice that of Co-CH$_3$ under identical conditions. In situ infrared spectroelectrochemistry identifies a metallocarboxylic intermediate and a cobalt–carbonyl species, indicating that C–OH bond cleavage occurs after CO_2 binding. Density functional theory calculations show that the pendant amine hydrogen-bonds to the bound CO_2 unit and assists intramolecular proton transfer during C–OH cleavage, thereby lowering the barrier for this step. Together, these results establish a clear mechanistic link between the positioned amine and the enhanced electrocatalytic performance, highlighting the value of second-sphere hydrogen-bond donors in the rational design of molecular catalysts for CO_2 reduction.



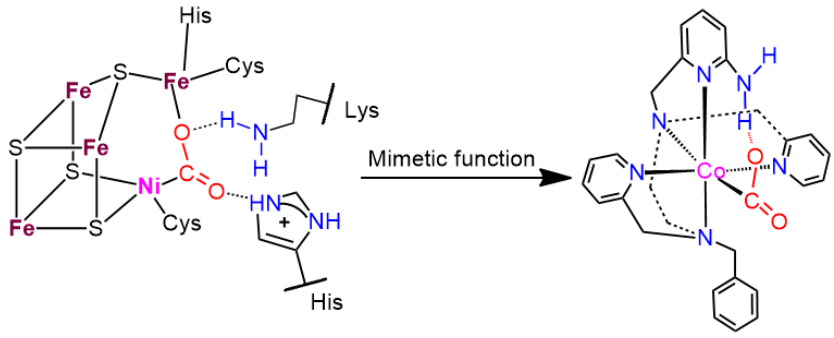
Keywords: Cobalt complex, Second coordination sphere, Electrocatalysis, CO_2 reduction

1. Introduction

Carbon dioxide, as an abundant, economical, and renewable C1 feedstock, has garnered significant attention for its catalytic conversion into liquid fuels-a process that could profoundly influence the global CO_2 balance [1, 2]. Electrochemical CO_2 reduction offers a promising pathway toward this goal by utilizing sustainable energy sources [3, 4]. However, significant kinetic and thermodynamic barriers associated with activating the stable CO_2 molecule remain major challenges. Thus, developing catalysts that promote CO_2 reduction at moderate potentials with high activity and strong selectivity over the competing hydrogen evolution reaction represents a critical research focus [5, 6]. In nature, the enzyme CO dehydrogenase (CODH), which features multi-metallic active sites, selectively and reversibly catalyzes the conversion of CO_2, protons, and reducing equivalents to CO (Scheme 1) [7]. In the catalytic cycle of Ni,Fe-CODH, X-ray diffraction studies have characterized an intermediate in which a CO_2-derived fragment bridges the Ni and Fe centers. High-resolution structural analysis reveals that CO_2 binds to Ni and Fe via the carbon and one carboxylate oxygen atom, respectively, with cleavage of the C=O bond assisted by a precisely positioned hydrogen-bond donor in the second coordination sphere [8, 9]. Similarly, pendant amines in the second coordination sphere of [FeFe]-hydrogenase are known to facilitate proton transfer and H_2 formation [10, 11]. These bioinspired motifs have inspired the design of metal complexes incorporating functional groups to promote catalytic CO_2 reduction at the metal center [12]. For example, Fe-porphyrin complexes show significantly enhanced performance when amide pendants are introduced at specific positions on the phenyl rings, underscoring the importance of precise positioning in the electrocatalytic conversion of CO_2 to CO [13]. Manganese bipyridine complexes bearing pendant amine also exhibit high activity and selectivity for CO_2 reduction [14]. Studies on cobalt complexes supported by aminopyridine macrocycles with varied pendant amine substitutions indicate that the secondary amine NH moiety plays a crucial role in catalyzing CO_2 reduction [15]. Mechanistic and density functional theory

studies on [CpCo(PR$_2$NR′$_2$)I]I confirm that second-sphere amine groups stabilize key intermediates through hydrogen bonding during hydride transfer from cobalt to CO_2 [16]. Similar secondary-sphere functional designs have proven effective in other electrocatalytic processes, such as the hydrogen evolution reaction (HER) and oxygen evolution reaction (OER) [17]. The strategic incorporation and spatial arrangement of proton-relay groups thus emerge as a crucial factor in enhancing electrocatalytic CO_2 reduction.

Inspired by bioinorganic models and analogous molecular catalysts, we designed a novel cobalt tripyridine-diamine complex (**Co-NH$_2$**) incorporating a strategically positioned intramolecular secondary amine moiety. A methyl-substituted analogue (**Co-CH$_3$**), functionalized at the equivalent position, was also synthesized for comparative evaluation. Experimental evidence confirms that this secondary amine acts as a hydrogen-bond donor to facilitate CO_2 binding and activation, as outlined in Scheme 1.



Scheme 1. The active site of Ni–Fe CO–dehydrogenase, showing activated CO_2 and the nearby network of hydrogen bond donor amino acid residues, provides inspiration for design of cobalt tripyridine-diamine complex featuring an amine in this work.

2. Materials and Methods

2.1 Synthesis

N-benzyl-N’-6-aminopyridinyl-2-methyl-N,N'-bis(pyridinyl-2-methyl)ethane-1,2-diamine (**L-**

NH_2) and N-benzyl-N'-6-methylpyridinyl-2-methyl-N,N'-bis(pyridinyl-2-methyl)ethane-1,2-diamine (**L-CH_3**) were prepared according to literature procedures (Figure S1) [18, 19]. The synthetic routes to complexes $[Co^{III}$(**L-NH_2**)OH$](BF_4)_2$ **(Co-NH_2)** and $[Co^{II}$(**L-CH_3**)MeCN$](BF_4)_2$ **(Co-CH_3)** are illustrated in Figure S2. $Co(BF_4)_2 \cdot 6H_2O$ (0.50 mmol) was added to an acetonitrile solution (5 mL) of **L-NH_2** or **L-CH_3** (0.50 mmol). The mixture was stirred at room temperature for 6 hours, after which the resulting solution was transferred into glass tubes. These tubes were placed in a flask containing diethyl ether, yielding block-shaped crystals of the respective complexes.

2.2 Electrochemistry

Cyclic voltammetry was performed using a CHI 630D potentiostat in a standard three-electrode cell under an inert (Ar) or CO_2 atmosphere. A glassy carbon disk (3 mm diameter) served as the working electrode, an $Ag/AgNO_3$ electrode as the reference electrode, and a platinum wire as the counter electrode. The supporting electrolyte was 0.1 M *n*-Bu_4NPF_6 in anhydrous CH_3CN, which was thoroughly degassed by bubbling dry Ar or CO_2 for at least 10 minutes prior to each experiment. All potentials were internally referenced to the ferrocenium/ferrocene ($Fc^{+/0}$) redox couple and are reported versus $Fc^{+/0}$. Bulk electrolysis was performed in a custom two-compartment cell (25 mL total volume). The working electrode was a carbon plate (surface area: 2 cm^2), with an $Ag/ AgNO_3$ pseudo-reference electrode and a Pt-mesh counter electrode; the counter compartment was isolated by a porous glass frit. All electrolyses were conducted in MeCN containing 0.1 M *n*-Bu_4NPF_6 as the supporting electrolyte. Prior to each experiment, the electrolysis solution was purged with CO_2 for 30 minutes.

2.3 IR-SEC

Spectroelectrochemical (SEC) measurements were carried out using a Bruker V80 FTIR spectrometer fitted with an MCT-A detector, while the electrode potential was regulated by a CHI 630D potentiostat. Measurements were performed in a home-built three-neck cell with CO_2-saturated

CH_3CN as the solvent. The working electrode was a glassy carbon disk (10 mm diameter), and the counter electrode was a platinum foil. An Ag/Ag^+ reference electrode, together with the target complex and 0.1 M *n*-Bu_4NPF_6 in CH_3CN, was housed within the SEC cell. Infrared spectra were collected in single-beam mode at a spectral resolution of 2 cm^{-1} or 4 cm^{-1}. Differential absorption spectra were obtained by referencing each spectrum to a background spectrum recorded immediately prior to potential application.

2.4 Computational Methods

All DFT computations were calculated at the B3LYP (the Becke three-parameter Lee-Yang-Parr hybrid functional) level using 6-31G(d) basis set for all atoms via Gaussian 09 program package [20, 21]. All structures were fully optimized and confirmed as minima by analytical vibrational frequency calculations with B3LYP/6-31G(d). The solvent acetonitrile was modeled as a dielectric continuum using polarizable continuum model (PCM). The basis sets and solvent model have been adopted to predict Co coordinates [22]. All calculated structures were visualized by Gauss View 5.0.9.

3 Results and discussion

3.1 Synthesis and Characterization

The two target tripyridine-diamine ligands, bearing amino (**L-NH_2**) and methyl (**L-CH_3**) substituents at the equivalent position respectively, were synthesized via an adapted literature procedure (Figure S1), with ^{1}H-NMR characterization results shown in Figure S3-S4 [18, 19]. The corresponding mononuclear cobalt complexes, **Co-NH_2** and **Co-CH_3**, were then prepared by reacting $Co(BF_4)_2 \cdot 6H_2O$ with **L-NH_2** and **L-CH_3** in acetonitrile at room temperature under ambient atmosphere, yielding nearly quantitative amounts (Figure S2). Complex **Co-NH_2** was obtained as a red crystalline solid, whereas **Co-CH_3** exhibited a reddish-brown color. Although both complexes were synthesized under identical conditions, **Co-NH_2** tends to adopt a trivalent cobalt oxidation state. This is supported by ^{1}H NMR spectroscopy, which shows sharp peak splitting for ligand protons,

consistent with a low-spin Co(III) center (Figure S5). The composition of **Co-CH₃** was verified by high-resolution mass spectrometry, with results in excellent agreement with the proposed formulations (Figure S6).

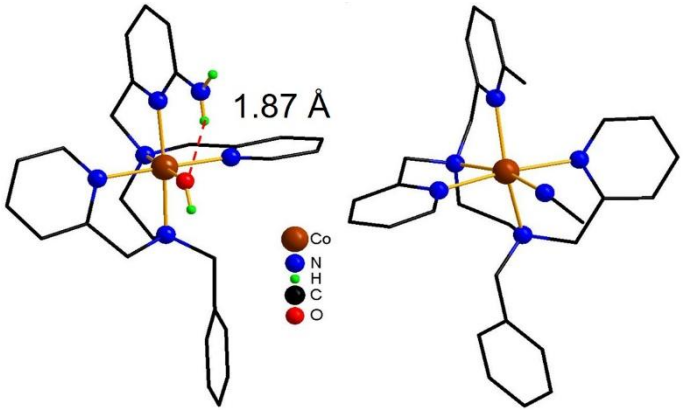


Figure 1. The solid-state structure of $[Co^{III}(\textbf{L-NH}_2)OH](BF_4)_2$ (**Co-NH₂**, left) and $[Co^{II}(\textbf{L-CH}_3)MeCN](BF_4)_2$ (**Co-CH₃**, right). Hydrogen atoms, noncoordinating ions, and solvent molecules are omitted for clarity.

Single-crystal XRD analyses of the two complexes, **Co-NH₂** and **Co-CH₃**, confirm that they share an identical cobalt tripyridine-diamine parent structure, differing only in their appended substituents (Figure 1). Both complexes exhibit a distorted octahedral coordination geometry, with BF_4^- counterions located outside the coordination sphere. In complex **Co-NH₂**, a hydroxyl ligand is coordinated to the cobalt center, and an intramolecular N–H···O hydrogen bond is observed in the solid state. As anticipated, the amine group is oriented in a manner that enables it to function as a hydrogen-bond donor toward CO_2-bound intermediates during catalysis. In contrast, complex **Co-CH₃** features a solvent molecule coordinated to the divalent cobalt center. Crystallographic data and refinement parameters are summarized in Table S1.

3.2 Electrochemistry

The electrochemical behavior of complex **Co-NH₂** was investigated by cyclic voltammetry (CV) in acetonitrile under an argon atmosphere with 0.1 M *n*-Bu_4NPF_6 as the supporting electrolyte. As

shown in Figure 2a and Figure S7, the CV profile of **Co-NH$_2$** exhibits a quasi-reversible redox event at –0.52 V and an irreversible reduction wave near –2.25 V, with all potentials referenced to the ferrocene/ferrocenium couple ($Fc^{+/0}$). Control experiments confirmed that the ligand **L-NH$_2$** does not contribute to these redox processes (Figure S8). Based on the observed potentials and electrochemical reversibility, the wave at –0.52 V is assigned to the Co^{III}/Co^{II} redox couple, while the irreversible reduction at –2.25 V is attributed to the Co^{II}/Co^{I} process. Upon addition of methanol to an Ar-saturated acetonitrile solution, the irreversible reduction wave at –2.25 V shifted positively with increasing methanol concentration, exhibiting a linear dependence on the logarithm of [CH_3OH] (Figure 2a, S9). This positive shift in potential indicates that the dissociation of the coordinated hydroxyl group is thermodynamically more favorable in the presence of a proton source, which is consistent with a concerted proton-electron transfer mechanism. However, the corresponding cathodic peak current did not increase significantly with methanol concentration, suggesting that the reaction remains limited by the initial metal-centered reduction under Ar. When the Ar-saturated methanol-containing solution was subsequently saturated with CO_2, a pronounced catalytic current enhancement (~10-fold) was observed at potentials approximately 300 mV positive to the Co^{II}/Co^{I} couple (Figure 2b). Control experiments in the absence of the catalyst confirmed that neither the glassy carbon electrode nor direct proton reduction contributes to the observed current increase (Figure S10). The results imply that the electrogenerated Co^{I} species binds CO_2 and initiates electrocatalytic reduction. Further introduction of methanol into the CO_2-saturated solution led to a linear increase in catalytic current with methanol concentration (Figure 2b), indicating that proton availability strongly modulates the catalytic rate. Moreover, the catalytic peak current (i_{cat}) scaled linearly with catalyst concentration, supporting a CO_2 reduction mechanism that is first-order in catalyst (Figure S11). Isotope experiments using CH_3OD as an alternative Brønsted acid source revealed slower current growth under CO_2 saturation (Figure S12), indicative of isotope-dependent dynamics for proton/deuteron delivery or transfer. A

controlled potential electrolysis (CPE) experiment conducted on the **Co-NH₂** complex at –2.25 V under CO_2 atmosphere and in the presence of 1.25 M methanol revealed that CO and H_2 were the primary products. The faradaic efficiency of CO is approximately 57% within 30 minutes and shows a gradually decreasing trend, dropping to 14% at 60 minutes (Figure S13). In addition, pronounced deposition was observed on the surface of the GC electrode after 60 min of electrolysis (Figure S14). XPS was employed to determine the chemical state of the species deposited on the glassy carbon (GC) electrode surface. As shown in Figure S15, the peak at 778.3 eV is assigned to metallic (zero-valent) cobalt, whereas the peaks at 781.4 and 784.3 eV arise from oxidized cobalt species. The relative peak areas indicate that metallic cobalt dominates the deposit formed under our electrolysis conditions. Published studies on other molecular catalysts have documented this behavior. The resulting deposited GC electrode was then used as the working electrode and poised at −2.25 V in a CO_2-saturated electrolyte containing methanol but no complex **Co-NH₂**. GC analysis showed that H_2 was the only detectable product. These results demonstrate that the deposited species are incapable of catalyzing CO_2 reduction and that their catalytic activity is limited to proton reduction to produce H_2. The species actually responsible for the conversion of CO_2 to CO are therefore complex **Co-NH₂**.

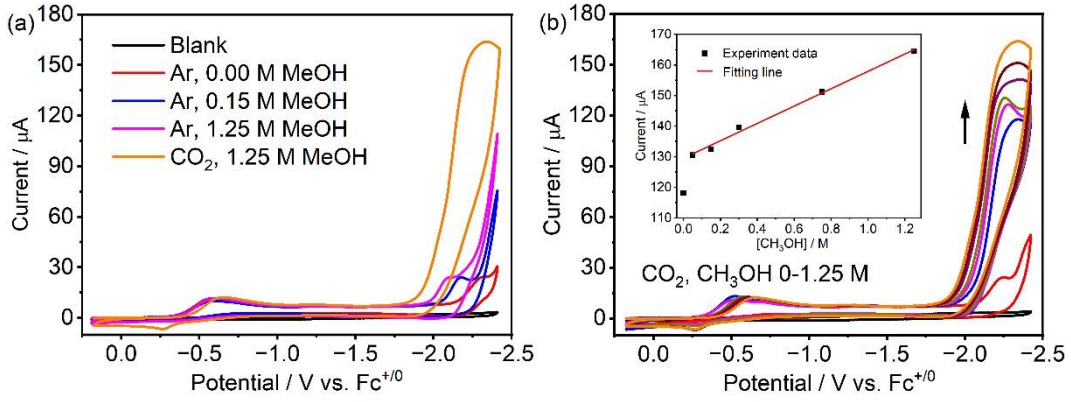


Figure 2. Cyclic voltammograms (CVs) showing the electrocatalytic reduction of CO_2 by 1 mM $[Co^{III}(\mathbf{L\text{-}NH_2})OH](BF_4)_2$ (**Co-NH₂**) in 0.1 M *n*-Bu_4NPF_6/MeCN. (a) The solution is under an atmosphere of Ar, then saturated with CO_2. (b) The solution is saturated with CO_2 with varied amounts of MeOH (0.05, 0.15, 0.3, 0.75, 1.25 M). Inset: the linear dependence of the catalytic currents on the

methanol concentration. Voltammograms are taken at a scan rate of 100 mV/s.

To elucidate the influence of the amine on catalytic behavior, the electrochemical properties of **Co-CH₃**, which features a methyl group, were investigated under conditions identical to those used for complex **Co-NH₂**. .As shown in Figure S16, the $Co^{II/I}$ redox couple of **Co-CH₃** occurs at approximately –1.75 V, which is about 500 mV more positive than that of complex **Co-NH₂**. Complex **Co-CH₃** also exhibits electrocatalytic activity toward CO_2 reduction (Figures S17–S19). However, unlike complex **Co-NH₂**, catalysis with **Co-CH₃** requires a prior reduction step to initiate, and under identical conditions its catalytic peak current is approximately 30 μA lower than that of **Co-NH₂**. As observed for complex **Co-NH₂**, the CPE experiment on complex **Co-CH₃** under a CO_2 atmosphere in the presence of 1.25 M methanol shows that CO and H_2 are the main products, accompanied by pronounced deposition of zero-valent cobalt and oxidized cobalt species on the GC electrode surface (Figure S20-S22). However, its CO faradaic efficiency within 30 min is only 30%, half that of complex **Co-NH₂**. These observations indicate that complexes **Co-NH₂** and **Co-CH₃** follow distinct pathways for electrocatalytic CO_2 reduction. Based on analogy with previous work by Grills et al., C–OH bond cleavage is proposed to be the rate-determining step, and a protonation-first mechanism is suggested [23]. In this context, the secondary amine is hypothesized to facilitate this bond cleavage, and this assumption is further explored by theoretical calculations, which indicate the involvement of the amine in two critical stages of the CO_2 reduction process. First, after CO_2 binds to the reduced cobalt center, the resulting adduct is stabilized by a hydrogen bond (NH···OCO = 1.720 Å) between the amine and one oxygen atom of the bound CO_2 (Figure S23). More importantly, during the subsequent dehydration of the carboxylic acid intermediate, the amine actively mediates an intramolecular proton transfer to guide hydroxy group dissociation (Figure 3 and S24–S25). The proposed pathway is supported by DFT calculations, which reveal a pronounced elongation of the C–

OH bond from 1.3449 Å to 1.399 Å, alongside a concurrent approach of the –OH and –NH_2 groups from 2.759 Å to 2.123 Å. These structural variations plausibly describe the reaction trajectory facilitated by the secondary amine.

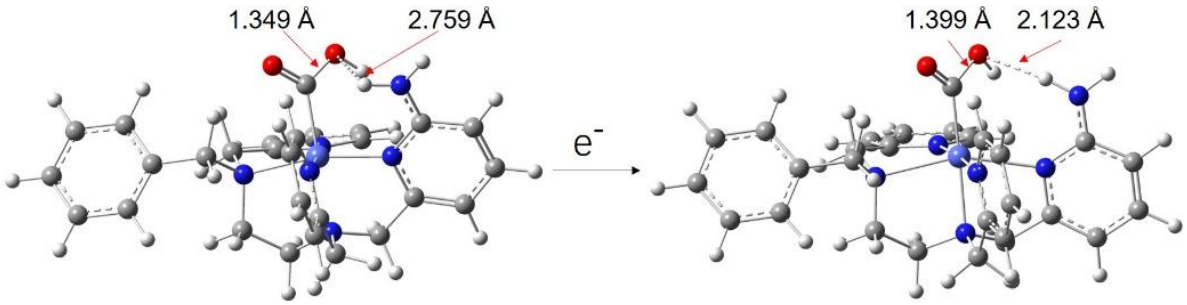


Figure 3. Optimized geometries of $[Co^{III}(\mathbf{L\text{-}NH_2})–COOH^-]^{2+}$ and $[Co^{II}(\mathbf{L\text{-}NH_2})–COOH^-]^{+}$ for the intramolecular hydrogen bond interaction. Co (light blue), C (gray), N (blue), O (red). Bond lengths are shown in Angstroms.

3.3 Spectroelectrochemistry

To investigate the subsequent reduction process following CO_2 binding, *in-situ* infrared spectroelectrochemical (IR-SEC) measurements were conducted. In the absence of CO_2, complex **Co-NH_2** in 1 M methanol/acetonitrile solution exhibits no distinct IR absorption modes of significant intensity between 1500 and 2500 cm^{-1}, even when the applied potential is varied from –1.0 to –2.4 V. Upon saturating the solution with CO_2, the differential IR-SEC spectrum of **Co-NH_2** reveals consumption of CO_2 at approximately 2340 cm^{-1}, along with the emergence of three carbonyl bands at 1903, 1669, and 1295 cm^{-1} starting from –1.9 V (vs. $Fc^{+/0}$, Figure 4). The absorption at 1903 cm^{-1} is assignable to the species $[Co^{+}(\mathbf{L\text{-}NH_2})–CO]^{+}$. This assignment is consistent with previously reported data, taking into account the electronic influence of the ligand [24]. The bands near 1669 and 1295 cm^{-1} are assigned to the C=O and C–OH stretching vibrations, respectively, and are associated with the metallocarboxylic intermediate in $[Co^{III}(\mathbf{L\text{-}NH_2})–COO^-]^{+}$, in which the amine proton hydrogen-bonds to the activated CO_2 [25]. In the presence of methanol, complex **Co-CH_3**

exhibits similar absorption bands (1909, 1663, and 1290 cm^{-1}; Figure S22) to those of complex **Co-NH₂**. The slight shift of the band around 1290 cm^{-1} to higher wavenumbers for complex **Co-NH₂** may be attributed to intramolecular hydrogen bonding, as discussed earlier. These IR-SEC results indicate that the decorated amine group can alter the pathway for C–OH bond cleavage from the metallocarboxylic intermediate.

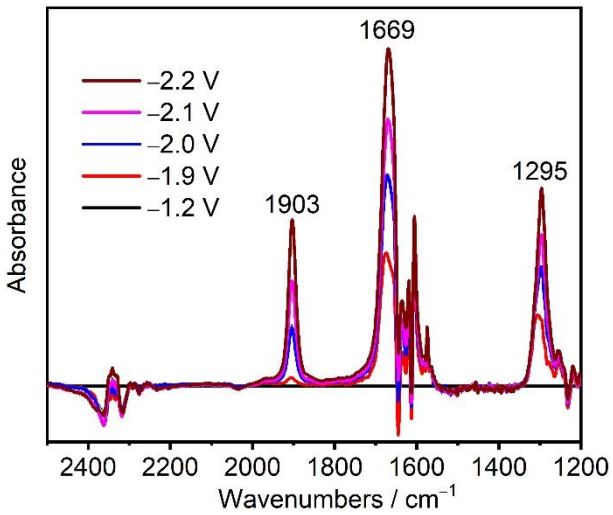
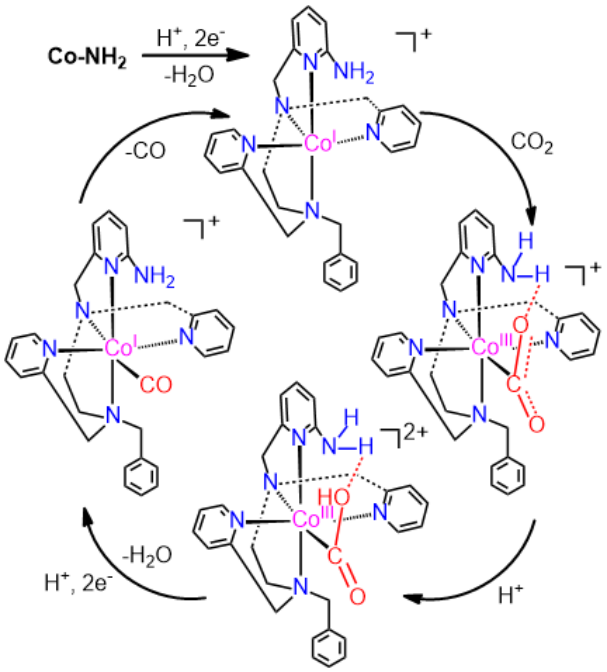


Figure 4. Differential IR-SEC spectrum of **Co-NH₂** (10.0 mM) recorded after electrolysis at varied potential from –1.9 to –2.2 V (vs. $Fc^{+/0}$) for 10 s in CO_2 saturated CH_3CN solution in the presence of 1 M CH_3OH. The tests are performed in CH_3CN with 0.1 M $^nBu_4NPF_6$ as the supporting electrolyte.

3.4 Catalytic cycle

A proposed mechanism for the electrocatalytic reduction of CO_2 to CO mediated by the **Co-NH₂** complex is outlined in Scheme 2. The process initiates with a two-electron reduction of the **Co-NH₂** species, yielding the active $[Co^{I}(\mathbf{L\text{-}NH_2})]^+$ intermediate. Introduction of CO_2 results in a pronounced positive shift in the $Co^{II/I}$ reduction potential and a substantial current enhancement in the corresponding potential region, consistent with an EC (electron transfer–chemical reaction) mechanism. This behavior suggests that $[Co^{I}(\mathbf{L\text{-}NH_2})]^+$ binds CO_2 following the $Co^{II/I}$ reduction, forming the $[Co^{III}(\mathbf{L\text{-}NH_2})\text{–}CO_2^{2-}]^+$ adduct. Notably, Fujita and co-workers previously identified

intramolecular hydrogen bonding between coordinated CO_2 and a macrocyclic ligand in solution [26]. In an analogous manner, we propose that the decorated $–NH_2$ group stabilizes the CO_2 unit in $[Co^{III}(\mathbf{L\text{-}NH_2})–CO_2^{2-}]^+$ via intramolecular hydrogen bonding. This interpretation is corroborated by the similarity between the IR spectroscopic features of $[Co^{III}(\mathbf{L\text{-}NH_2})–CO_2^{2-}]^+$ and those reported for the $[Co^{III}(\text{macrocycle})–CO_2^{2-}]^+$ species. Under acidic conditions, $[Co^{III}(\mathbf{L\text{-}NH_2})–CO_2^{2-}]^+$ undergoes protonation via an external proton source to afford a metallocarboxylic (M–COOH) intermediate. Subsequent reduction, facilitated by the pendant amine group, promotes C–OH bond cleavage, leading to a carbonyl complex that releases CO and regenerates the $[Co^{+}(\mathbf{L\text{-}NH_2})]^+$ catalyst, thereby completing the catalytic cycle.



Scheme 2. A proposed mechanism for the reduction of CO_2 mediated by **Co-NH₂.**

4 Conclusions

In summary, a novel cobalt tripyridine-diamine complex (**Co-NH₂**) featuring a strategically positioned intramolecular secondary amine group has been synthesized. Electrochemical evaluation under CO_2-saturated conditions in the presence of methanol demonstrates that **Co-NH₂** operates via

a proton-coupled electron transfer pathway, exhibiting an enhanced catalytic current relative to its methyl-substituted analogue (**Co-CH_3**), which was prepared for comparative assessment. Spectroelectrochemical and density functional theory studies have confirmed that the amine group, which functions as the second coordination sphere, acts as an intramolecular hydrogen-bond donor that stabilizes CO_2 binding and promotes C–OH bond cleavage during the electrocatalytic reduction of CO_2, thereby establishing a reaction pathway that fundamentally differs from the one followed by the methyl-substituted control system.

Funding

This work was supported by Guangdong Basic and Applied Basic Research Foundation (2022A1515110778, 2023A1515140150), Huizhou Excellent Science and Technology Talent Project (2023EQ050036), National Natural Science Foundation of China (22101186).

Conflict of Interest

The authors declare no conflict of interest.

Data Availability Statement

The data that support the findings of this study are available in the Supporting Information.

Author Contribution

Conceptualization: Y.Y., J.Y. Investigation: Y.Y., Y.F. Validation: Y.F., Y.Y, M.L. Formal analysis: Z.Z., Y.L., J.J., H.W., Writing—original draft preparation: Y.Y., G.L. Writing—review and editing: Y.Y., H.Y.

References

1. Keith DW, Holmes G, St Angelo D, Heidel K (2018) A process for capturing CO_2 from the atmosphere. Joule 2:1573–1594. https://doi.org/10.1016/j.joule.2018.05.006.
2. Hu XM, Liang HQ, Rosas-Hernández A, Daasbjerg K (2025) Electrochemical valorization of captured CO_2: recent advances and future perspectives. Chem Soc Rev 54:1216–1250.

https://doi.org/10.1039/D4CS00480A.

3. Bushuyev OS, De Luna P, Dinh CT, Tao L, Saur G, van de Lagemaat J, Kelley SO, Sargent EH (2018) What should we make with CO_2 and how can we make it? Joule 2:825–832. https://doi.org/10.1016/j.joule.2017.09.003.
4. Jiang M, Wang H, Zhu M, Luo X, He Y, Wang M, Wu C, Zhang L, Li X, Liao X et al (2024) Review on strategies for improving the added value and expanding the scope of CO_2 electroreduction products. Chem Soc Rev 53:5149–5189. https://doi.org/10.1039/D3CS00857F.
5. Franco F, Rettenmaier C, Jeon HS, Roldan Cuenya B (2020) Transition metal-based catalysts for the electrochemical CO_2 reduction: from atoms and molecules to nanostructured materials. Chem Soc Rev 49:6884–6946. https://doi.org/10.1039/D0CS00835D.
6. Elgrishi N, Chambers MB, Wang X, Fontecave M (2017) Molecular polypyridine-based metal complexes as catalysts for the reduction of CO_2. Chem Soc Rev 46:761–796. https://doi.org/10.1039/C5CS00391A.
7. Hu Z, Spangler NJ, Anderson ME, Xia J, Ludden PW, Lindahl PA, Münck E (1996) Nature of the C-cluster in Ni-containing carbon monoxide dehydrogenases. J Am Chem Soc 118:830–845. https://doi.org/10.1021/ja9528386.
8. Jeoung JH, Dobbek H (2007) Carbon dioxide activation at the Ni,Fe-cluster of anaerobic carbon monoxide dehydrogenase. Science 318:1461–1464. https://doi.org/10.1126/science.1148481.
9. Mondal B, Song J, Neese F, Ye S (2015) Bio-inspired mechanistic insights into CO_2 reduction. Curr Opin Chem Biol 25:103–109. https://doi.org/10.1016/j.cbpa.2014.12.022.
10. Kleinhaus JT, Wittkamp F, Yadav S, Siegmund D, Apfel UP (2021) [FeFe]-Hydrogenases: maturation and reactivity of enzymatic systems and overview of biomimetic models. Chem Soc Rev 50:1668–1784. https://doi.org/10.1039/D0CS01089H.
11. Thammavongsy Z, Mercer IP, Yang JY (2019) Promoting proton coupled electron transfer in

redox catalysts through molecular design. Chem Commun 55:10342–10358. https://doi.org/10.1039/C9CC05139B.

12. Amanullah S, Saha P, Nayek A, Ahmed ME, Dey A (2021) Biochemical and artificial pathways for the reduction of carbon dioxide, nitrite and the competing proton reduction: effect of 2nd sphere interactions in catalysis. Chem Soc Rev 50:3755–3823. https://doi.org/10.1039/D0CS01405B.
13. Gotico P, Boitrel B, Guillot R, Sircoglou M, Quaranta A, Halime Z, Leibl W, Aukauloo A (2019) Second-sphere biomimetic multipoint hydrogen-bonding patterns to boost CO_2 reduction of iron porphyrins. Angew Chem Int Ed 58:4504–4509. https://doi.org/10.1002/anie.201814339.
14. Rønne MH, Cho D, Madsen MR, Jakobsen JB, Eom S, Escoudé É, Hammershøj HCD, Nielsen DU, Pedersen SU, Baik MH et al (2020) Ligand-controlled product selectivity in electrochemical carbon dioxide reduction using manganese bipyridine catalysts. J Am Chem Soc 142:4265–4275. https://doi.org/10.1021/jacs.9b11806.
15. Chapovetsky A, Welborn M, Luna JM, Haiges R, Miller TF III, Marinescu SC (2018) Pendant hydrogen-bond donors in cobalt catalysts independently enhance CO_2 reduction. ACS Cent Sci 4:397–404. https://doi.org/10.1021/acscentsci.7b00607.
16. Roy S, Sharma B, Pécaut J, Simon P, Fontecave M, Tran PD, Derat E, Artero V (2017) Molecular cobalt complexes with pendant amines for selective electrocatalytic reduction of carbon dioxide to formic acid. J Am Chem Soc 139:3685–3696. https://doi.org/10.1021/jacs.6b11474.
17. Barrio J, Pedersen A, Favero S, Luo H, Wang M, Sarma SC, Feng J, Ngoc LTT, Kellner S, Li AY et al (2023) Bioinspired and bioderived aqueous electrocatalysis. Chem Rev 123:2311–2348. https://doi.org/10.1021/acs.chemrev.2c00429.
18. Zhang P, Wang M, Gloaguen F, Chen L, Quentel F, Sun L (2013) Electrocatalytic hydrogen evolution from neutral water by molecular cobalt tripyridine–diamine complexes. Chem Commun

49:9455–9457. https://doi.org/10.1039/c3cc43491e.

19. Chen L, Li X, Ren G, Zhang P, Wang N (2020) Bioinspired design of positioned amine assists hydrogen evolution from neutral water by nickel tripyridine-diamine. ChemCatChem 12:3853–3856. https://doi.org/10.1002/cctc.202000100.
20. Becke AD (1993) A new mixing of Hartree–Fock and local density-functional theories. J Chem Phys 98:1372–1377. https://doi.org/10.1063/1.464304.
21. Lee C, Yang W, Parr RG (1988) Development of the Colle-Salvetti correlation-energy formula into a functional of the electron density. Phys Rev B 37:785–789. https://doi.org/10.1103/PhysRevB.37.785.
22. Chen L, Guo Z, Wei XG, Gallenkamp C, Bonin J, Anxolabéhère-Mallart E, Lau KC, Lau TC, Robert M (2015) Molecular catalysis of the electrochemical and photochemical reduction of CO_2 with earth-abundant metal complexes. Selective production of CO vs HCOOH by switching of the metal center. J Am Chem Soc 137:10918–10921. https://doi.org/10.1021/jacs.5b06535.
23. Ngo KT, McKinnon M, Mahanti B, Narayanan R, Grills DC, Ertem MZ, Rochford J (2017) Turning on the protonation-first pathway for electrocatalytic CO_2 reduction by manganese bipyridyl tricarbonyl complexes. J Am Chem Soc 139:2604–2618. https://doi.org/10.1021/jacs.6b08776.
24. Zhang W, Luo ZM, Lin HW, Wang JW (2025) Chelation numbers differentiate performances of Co(II) macrocyclic catalysts in electro-photocatalytic CO_2 reduction. Chem Asian J 20:e00373. https://doi.org/10.1002/asia.202500373.
25. Froehlich JD, Kubiak CP (2015) The homogeneous reduction of CO_2 by $[Ni(cyclam)]^+$: increased catalytic rates with the addition of a CO scavenger. J Am Chem Soc 137:3565–3573. https://doi.org/10.1021/ja512575v.
26. Fujita E, Creutz C, Sutin N, Brunschwig BS (1993) Carbon dioxide activation by cobalt

macrocycles: evidence of hydrogen bonding between bound CO_2 and the macrocycle in solution. Inorg Chem 32:2657–2662. https://doi.org/10.1021/ic00064a015.

Supplementary Files

This is a list of supplementary files associated with this preprint. Click to download.

- catalysisletterSIBioinspiredDesignofProximalAmineBoostsElectrocatalyticReductionofCO2byCobaltTripyridineDiamineComplex.docx